Study of the Velocity and Direction of Piezoelectric Robot Driven by Traveling Waves

Jie Zhao,Senior Member, IEEE, Guanyu Mu, Huijuan Dong, Tong Sun and Kenneth.T.V. Grattan

***Abstract*—Self-running piezoelectric robots have the advantages of being low cost, high load ratio and fast speed of operation, as well as showing few limitations in confined spaces or for underwater applications. Controlling the speed of motion of such robots by adjusting the Standing Wave Ratio (SWR) along the vibration plate of the robot is important. Compared to the conventional dual-mode excitation method which is based on the adjustment of the excitation frequency, *f*, a novel SWR-based control method, using the adjustment of the temporal phase shift, *θ*, has been first derived by the authors. It has been found that the travelling wave component could be maximised using both methods, either by setting the value of *f* to the root mean square of the two adjacent modal frequencies, or by programming *θ* to have a sum of π when added to the spatial phase difference. It can be seen that using the 'θ-based' traveling wave control method, smoother motion and higher resolution of the motion speed is achieved. In this research, by using the novel *θ*-based method to drive the robot, its motion characteristics, such as voltage-speed, load capacity and ability to move on different surface materials, have been tested through a series of experiments carried out and reported.**

***Index Terms*—self-running piezoelectric robot, dual-mode excitation method, temporal phase shift, adjacent modal frequencies, Standing Wave Ratio (SWR)**

I. Introduction

SELF-RUNNING piezoelectric robots have many potential applications for use in confined spaces [1], [2] or underwater [3]-[5], due to their favourable characteristics such as having a simple structure, being low cost to manufacture and having both a high load ratio and fast speed of operation, as well as no restrictions on the material on which they can walk. Compared to traditional robots with movable joints, piezoelectric robots generate neither strong electromagnetic radiation, nor produce undesired noise or dust in their operation. These advantages allow the self-running piezoeletric robot to have a potential amphibious ability that can enable it to "fly on the ground" – to do this on the ground with any material and to "dive in water" in a liquid medium.

The piezoelectric self-running robot can be driven by Standing Waves (SWs) or Traveling Waves (TWs), according to the type of vibrational waves used [6]. Leg-shaped or tooth-shaped structures (in the SW-type robot) are often mounted on a vibrating plate, to convert the vertical vibration on the plate to the horizontal motion of the robot, when it is walking on a surface [7]-[10]. This kind of leg-shaped or tooth-shaped structure, which resembles the design of many ultrasonic motors [11]-[16], is not only difficult to fabricate, but the position, shape, size and material properties of the leg or tooth will also affect the performance of the robot [17], [18]. In addition, the use of such leg-shaped or tooth-shaped structures means that SW-driven robots are not easy to miniaturize, and this restricts their potential range of applications. By comparison, TW-driven robots have no such limitations because of their simple structure – only one or more pairs of ceramic piezoelectric patches are glued at both ends of a vibrating plate [19]-[21]. Moreover, the robots are able to move faster when driven using the TWs, but it is essential, however, to efficiently excite and control the traveling waves to allow TW-driven robots to be developed further.

It has been reported that TWs can be generated using the Exciter-Absorber method or the Exciter-Exciter method [22]-[24]. The first of these, the Exciter-Absorber mode can be realized when a passive electric network is connected to one of the ceramic piezoelectric patches, glued to the vibrating plate, to absorb the energy. The circuit parameters required can be calculated using transmission line theory [25], [26]. However, this circuit not only produces heat, but also cannot be programmed to adjust both the TW component and its direction. An alternative method, the Exciter-Exciter mode can be used, allowing the direction and amplitude of the TWs to be adjusted by programming the excitation frequency between the two adjacent modal frequencies (this is known as Dual-Mode Excitation) [27]-[31], at a fixed phase shift value (θ=90°). In this way, the direction and speed of the TW-driven robot could

The authors acknowledge the support of the National Natural Science Foundation of China (52275014) and the support of the British Council through the 'Going Global Partnerships - Enabling Grants to Strengthen UK-China Institutional Partnerships through academic collaboration 2021' program.

Jie Zhao, Guanyu Mu and Huijuan Dong are with the State Key Laboratory of Robotics and System, Harbin Institute of Technology, Harbin 150001, China (Corresponding author: Huijuan Dong (dhj@hit.edu.cn)).

Tong Sun and Kenneth.T.V. Grattan are with City, University of London, London, EC1V 0HB, UK (Corresponding author: Kenneth.T.V. Grattan (K.T.V.Grattan@city.ac.uk)).

be adjusted [32]-[34]. However, when the excitation frequency deviates from the modal frequency, the amplitude of vibration of the plate would drop rapidly as well, which makes it difficult to create smooth control of the robot speed.

In this study, an alternative method for programmable control of the direction and speed of a TW-based piezoelectric self-running robot, using the Exciter-Exciter mode, is described. Compared to the Dual-Mode Excitation method, only θ is changed using this approach, which allows better control of the direction and components of the TWs, at a fixed frequency [35], [36]. As a result, the motion of the self-running piezoelectric robot would be expected to be smoother than was seen when using the Dual-Mode Excitation method. In this work, the structural parameters of a piezoelectric self-running robot have first been optimized using simulation, following which a series of experiments has been carried out to demonstrate the method proposed for self-running piezoelectric robots.

II. Method for Adjusting the Direction of Motion of the Self-Running Piezoelectric Robot

A. Method to adjust the direction using the excitation frequency, f

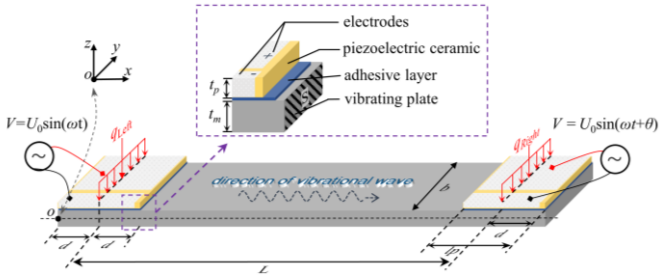

Fig. 1. Schematic of the self-running piezoelectric robot, used in the Exciter-Exciter mode. (The inset shows a close-up view of the piezoelectric ceramic attached to the substrate.)

Fig. 1 shows a schematic of the piezoelectric self-running robot developed in this work where two piezoelectric ceramic patches of length, l_p=2d, and width, b, were attached to a vibrating plate of length, (L+2d).

Here two electrical signals, having the same amplitude and frequency, U_0 and ω respectively, but with a phase shift, θ, are applied to the two piezoelectric patches (which are shown in yellow in Fig. 1). As a result, to simplify the model, the piezoelectric effect can be considered as producing two excitation forces $q_{Left}(x,t)$ and $q_{Right}(x,t)$, located in the middle of the piezoelectric patches in the x-direction, where these are shown in red in Fig. 1.

The equation for the displacement of the plate $w(x,t)$ (i.e., at time, t, and position, x) can be written and used to understand one-dimensional TWs along the x-direction of the piezoelectric self-running robot, where to do so, $w(x,t)$ could be determined by using Euler-Bernoulli beam theory:

$$EI\frac{\partial^4 w}{\partial x^4}+\rho S\frac{\partial^2 w}{\partial t^2}=q(x,t) \qquad (1)$$

where S is the cross-sectional area, ρ is the mass density per unit volume, I is the moment of inertia of S, and E represents Young's modulus of the vibrating plate. Assuming that $w(x,t)$ can be expanded in terms of the normal modes, $W(x)$ and general functions of time, $e^{j\omega t}$:

$$w(x,t)=W(x)e^{j\omega t}=\sum_{n=1}^{\infty}a_n W_n(x)e^{j\omega t} \qquad (2)$$

where a_n is the coefficient of displacement. $W_n(x)$ is the n-th order normal modes of the vibrating plate, and as a result its general solution can be written as:

$$W_n(x)=C_1\sin\beta x+C_2\cos\beta x+C_3\sinh\beta x+C_4\cosh\beta x,$$

$$\text{where } \beta^4=\frac{\rho S}{EI}\omega^2$$

where C_1, C_2, C_3, C_4 are four constants. Considering the existence of the piezoelectric patches used, the simple support boundary condition at both ends of the plate was applied to simplify the model (where x=0, and x=L+2d), the bending moment and displacement are equal to zero:

$$EI\frac{\partial^2 w(x,t)}{\partial x^2}\Big|_{x=0}=0 \qquad EI\frac{\partial^2 w(x,t)}{\partial x^2}\Big|_{x=L+2d}=0$$

$$w(x,t)\big|_{x=0}=0 \qquad w(x,t)\big|_{x=L+2d}=0$$

resulting in C_2=C_3=C_4=0, and so the normal modes, $W_n(x)$ of the vibrating plate are thus given by:

$$W_n(x)=C_1\sin(\beta_n x) \qquad (3)$$

It can be noted that $\beta_n=\sqrt[4]{\frac{\rho S}{EI}\omega_n^2}=\frac{n\pi}{L}$, (n=1, 2, …) by combining its definition and the boundary conditions in (3), where ω_n is the n-th mode angular frequency. Considering the position of the external forces shown in Fig. 1, the left and right excitation forces, $q_{Left}(x,t)$ and $q_{Right}(x,t)$, can be expressed as:

$$q_{left}(x,t)=A\delta(x-d)\sin\omega t$$

$$q_{right}(x,t)=A\delta(x-L+d)\sin(\omega t+\theta)$$

where A is the amplitude of the excitation force, δ is the Dirac function, and d = L_p/2, represents the center position of the piezoelectric patch in the x-direction (as can be seen in Fig.1). When the vibration is excited by $q_{Left}(x,t)$ and $q_{Right}(x,t)$, respectively, (1) can be solved by applying the modal superposition principle [33], [37]. As a result, the z-directional displacement of the vibrating plate, $w(x,t)$, can be rewritten as:

$$w(x,t)=\sum_{n=1}^{\infty}a_n\Big(\underbrace{\sin(\beta_n x)\sin\omega t}_{\text{Excited by } q_{Left}}+\underbrace{(-1)^n\sin(\beta_n x)\sin(\omega t+\theta)}_{\text{Excited by } q_{Right}}\Big) \qquad (4)$$

$$\text{where } a_n(x)=\frac{2A}{L}\frac{\sin\beta_n d}{EI(\beta_n^4-\beta^4)}$$

It is known from work previously reported in the literature that the excitation frequency, ω, can be adjusted using the Dual-Mode excitation method. Following the approach of (4), if only the superposition of two adjacent modes, the N-th, and the (N+1)-th is considered, while ignoring the effect of other modes, $w(x,t)$ can be simplified (assuming that N is an even number) as follows:

$$\begin{aligned}w(x,t)=&\Big[\underbrace{a_n\sin(\beta_n x)}_{\text{N}^{th}\text{ mode}}+\underbrace{a_{n+1}\sin(\beta_{n+1}x)}_{(\text{N+1})^{th}\text{ mode}}\Big]\sin\omega t\\&+\Big[\underbrace{a_n\sin(\beta_n x)}_{\text{N}^{th}\text{ mode}}-\underbrace{a_{n+1}\sin(\beta_{n+1}x)}_{(\text{N+1})^{th}\text{ mode}}\Big]\cos\omega t\end{aligned} \qquad (5)$$

noting that ω lies between two modal frequencies, $f_N = \frac{\omega_N}{2\pi}$ and $f_{N+1} = \frac{\omega_{N+1}}{2\pi}$, as shown in Fig. 2(a).

In order to separate the TW and SW terms, $w(x,t)$ in (5) can be rewritten as a mixture of SWs and TWs, $w(x,t)$ near the middle of the vibrating plate ($x \approx 0.5L$) can be simplified further, as shown below [33]:

$$w(x,t) = \underbrace{\sqrt{2}a_N \sin(\omega t - \frac{\beta_N + \beta_{N+1}}{2}x)}_{\text{TW part (x+ direction)}} + \underbrace{\sqrt{2}(a_N + a_{N+1})\sin(\beta_{N+1}x)\sin(\omega t - \frac{\pi}{4})}_{\text{SW part}} \quad (6)$$

Similarly, for the next pair of modes, the (N+1)-th (an even number) and the (N+2)-th, $w(x,t)$ is given by:

$$w(x,t) = \underbrace{\sqrt{2}a_{N+1} \sin(\omega t + \frac{\beta_{N+1} + \beta_{N+2}}{2}x)}_{\text{TW part (x- direction)}} + \underbrace{\sqrt{2}(a_{N+1} + a_{N+2})\sin(\beta_{N+2}x)\sin(\omega t - \frac{\pi}{4})}_{\text{SW part}} \quad (7)$$

It can be seen from both (6) and (7) that the direction of the TW changes if ω crosses any modal frequency, this also being shown in Fig. 2(a). Clearly, the TW component reaches its maximum when the coefficients of the part of the SWs in (6) and (7) are equal to 0, so then by combining this with (4), the frequencies of the TWs can be easily obtained as ω_{TW1}, and ω_{TW2}, in Fig. 2:

$$\beta_n^4 - \beta^4 = -(\beta_{n+1}^4 - \beta^4) \text{ i.e. } \omega_{TW1} = \sqrt{\frac{\omega_n^2 + \omega_{n+1}^2}{2}} \quad (8)$$

Equation (8) implies that the TW component is maximized when ω_{TW1}, and ω_{TW2} (marked in green in Fig. 2(a)) have the values of the root mean square of two adjacent modal frequencies. To further characterize the TW component of the flexural waves on the vibrating plate, the Standing Wave Ratio ($SWR = w_{\max} / w_{\min}$, where $w_{\max}$ and $w_{\min}$ are the maximum and minimum values of the amplitude of $w(x,t)$, respectively) is defined and used [38]. A smaller value of the SWR means a higher component of the TWs. Accordingly, the minimum value of the SWR approaches unity, indicating pure TWs. The relationship between the SWR and the excitation frequency, f, is shown in Fig. 2(a), where the modal frequencies were obtained from (3) under the conditions of n being equal to 10, 11, and 12, and the values of the SWR were calculated from (3) and (5) using a Matlab-programme.

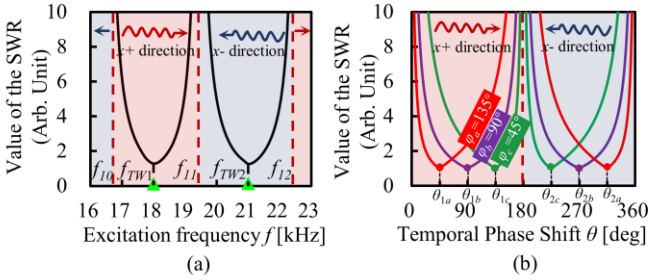

Fig. 2. Theoretical relationship (a) between the SWR and the excitation frequency, f, (b) between the SWR and the excitation phase shift, θ. (The dark blue and red colored areas represent the x+ and x- TW directions, respectively; in subgraph (a), f_{10}, f_{11}, f_{12} are three adjacent modal frequencies, 16.56kHz, 19.44kHz and 22.52kHz respectively; f_{TW1} and f_{TW2} are the two TW frequencies with opposite directions, 18.02 kHz and 21.01 kHz accordingly. in subgraph (b), θ_a=45° (red curve), θ_b=90° (purple curve) and θ_c=135° (green curve))

In conclusion, combining (6) and (7) with Fig. 2(a), this gives the vibrational distribution on the vibrating plate and denotes the relationship between the SWR and the excitation frequency, f. It can be seen that when f is equal to one of the modal frequencies (f_{10}, f_{11}, f_{12}), the value of the SWR is infinite, indicating that the pure SWs have been formed. By comparison, if f has the value of the root mean square of the two adjacent modal frequencies, a pure TW is formed. Moreover, when the value of f crosses one of the modal frequencies, the direction of the TW reverses. Therefore, it is theoretically possible to control the direction of motion by programming the value of f.

However, if f were adjusted between the two adjacent modal frequencies, not only would the value of the SWR change, but also the displacement amplitude would drop in an undesirable way. This causes the self-running robot to have low motional stability. The change of the f value would likely detune the piezoelectric patches and thus make the system inoperative. In order to solve this problem, the method of programming the excitation phase shift, θ, will be discussed below in Section 2.2, as a way to offer a high-resolution and smooth speed adjustment of the motion of the robot.

B. Method to adjust the direction using the excitation phase shift, θ

The distribution of the vibration on the vibrating plate can be seen as the superposition of two SWs, formed by two excitation forces, q_{Left} and q_{Right} [33], shown in Fig. 1. Specifically, the distance, L, between $q_{Left}(x,t)$ and $q_{Right}(x,t)$ must produce a spatial phase difference between the two SWs, given by $\varphi = k(L - n\lambda)$, where n is an integer, and λ and k are the vibrational wavelength and the wave number respectively. As a result, the displacement, $w(x,t)$, can be given by (9) [39]:

$$w(x,t) = \sum_{n=1}^{\infty} a_n [\sin(\beta x)\sin\omega t + \sin(\beta x + \varphi)\sin(\omega t + \theta)] \quad (9)$$

Following (9), the normalized maximum and minimum amplitudes of the displacement values, $\hat{w}_{max}$ and $\hat{w}_{min}$, can be derived and expressed as [40].

$$\hat{w}_{\max}(\theta,\varphi) = \max(2\left|\sin\frac{\varphi}{2}\sin\frac{\theta}{2}\right|, 2\left|\cos\frac{\varphi}{2}\cos\frac{\theta}{2}\right|)$$

$$\hat{w}_{\min}(\theta,\varphi) = \min(2\left|\sin\frac{\varphi}{2}\sin\frac{\theta}{2}\right|, 2\left|\cos\frac{\varphi}{2}\cos\frac{\theta}{2}\right|)$$

Therefore, the SWR can be derived as:

$$SWR = \frac{\max(2\left|\sin\frac{\varphi}{2}\sin\frac{\theta}{2}\right|, 2\left|\cos\frac{\varphi}{2}\cos\frac{\theta}{2}\right|)}{\min(2\left|\sin\frac{\varphi}{2}\sin\frac{\theta}{2}\right|, 2\left|\cos\frac{\varphi}{2}\cos\frac{\theta}{2}\right|)} \quad (10)$$

The relationship between the SWR and θ is plotted in Fig. 2(b), where the different colored curves represent the three nonidentical values of φ. It can be seen from Fig. 2 (b) that the pure TW can be formed at the two temporal phase shifts, θ_1 and θ_2, which are symmetric about π for each value of φ. It is noted that under the condition where the value of the SWR is unity, θ_1 and θ_2 are related to φ as follows:

$$\varphi = \begin{cases} \pi - \theta_1 = \theta_2 - \pi & 0 \le \varphi < \pi \\ \pi + \theta_1 = 3\pi - \theta_2 & \pi \le \varphi < 2\pi \end{cases} \quad (11)$$

In addition, if the temporal phase shifts were programmed to θ_1 or θ_2, the two TWs would be induced in the opposite direction along the vibrating plate of the robot, with these TWs being expressed as :

$$\hat{w}(x,t)=\sin\varphi\sin(\pm\omega t-kx+\theta) \quad (12)$$

As can be seen from (11) and (12), not only is the direction of the TWs affected by the spatial phase difference, φ, but the amplitude of the wave is also closely connected to φ. To achieve the maximum amplitude of the TW, the optimised value of φ is 90° and 270°. Thus, under the condition that φ was given and fixed, both the direction and amplitude of the TWs could be adjusted through programming the value of θ, and as a result the motion of the robot can be controlled.

III. Structural Design of the Self-Running Piezoelectric Robot

To optimize the structural design of the self-running piezoelectric robot, Finite Element (FE) analysis was used to determine the critical structural parameters of the prototype, as well as the best material selection of each component used. The FE analysis was performed using the following software – Mechanical APDL (ANSYS Corporation, Canonsburg, PA, USA), and the piezoelectric material and the aluminum vibrating plate had the element type SOLID226 and SOLID186, respectively. The material parameters of the piezoelectric ceramic were given in Section III (B), and the damping coefficient was set to 0.003 [36].

A. The structural parameters of the vibrating plate

As illustrated in Fig. 1, the self-running robot is composed of a vibrating plate (shown in grey color) and two piezoelectric patches (shown in yellow color) which were pasted at the two ends, where the thickness of the adhesive layer was relatively small (and thus ignored in the FE model). Specifically, the length and thickness of the vibrating plate have the values of (L+2d) and t_m, while these values for the piezoelectric patches were l_p and t_p, respectively. Both structures of the robot share the same width, b. The thickness of the vibrating plate, t_m, was 0.5 mm, this being chosen to balance the weight and the stiffness of the prototype. Additionally, (L+2d) and b have values of 100 mm and 17 mm, to ensure the bending vibration mode only exists in the x-direction.

B. Optimization of the parameters of the piezoelectric patches

In order to build the FE model, the material properties of the robot were made identical to the actual physical parameters planned, and thus the materials comprising the vibrating plate were aluminum, steel and copper. The piezoelectric patches (type PZT-5A, series resonant frequency f_s being 48084.4Hz and 47418.3Hz, respectively, HongSheng Acoustic Electronic Equipment Co., Ltd., Baoding City, China) were excited to provide the vibration forces, $q_{Left}(x,t)$ and $q_{Right}(x,t)$. The elastic constant matrix, c, the piezoelectric constant matrix, e, and the relative dielectric constant matrix, ε, of the material PZT-5A are detailed, as shown in (13) below, respectively:

$$[c]=\begin{bmatrix} 12.72 & 8.02 & 8.47 & 0 & 0 & 0 \\ 8.02 & 12.72 & 8.47 & 0 & 0 & 0 \\ 8.47 & 8.47 & 11.74 & 0 & 0 & 0 \\ 0 & 0 & 0 & 2.30 & 0 & 0 \\ 0 & 0 & 0 & 0 & 2.30 & 0 \\ 0 & 0 & 0 & 0 & 0 & 2.35 \end{bmatrix} \times 10^{10}\, N/m^2$$

$$[e]=\begin{bmatrix} 0 & 0 & 0 & 0 & 17.03 & 0 \\ 0 & 0 & 0 & 17.03 & 0 & 0 \\ -6.62 & -6.62 & 23.24 & 0 & 0 & 0 \end{bmatrix} C/m^2 \qquad [\varepsilon]=\begin{bmatrix} 1704 & 0 & 0 \\ 0 & 1704 & 0 \\ 0 & 0 & 1434 \end{bmatrix}$$

It can be noted that the higher the vibrational displacement in the z-direction, the greater is the driving force at a given frequency. In order to make the robot move faster, the vibrational displacement in the z-direction was optimised by changing the values of t_p and l_p. In order to guarantee that the bending vibration along the x-direction is dominating and to avoid the vibration mode in the y-direction, l_p=35mm (l_p≈2b) was initially selected, prior to the determination of the thickness, t_p, after which the value of l_p was then scanned parametrically.

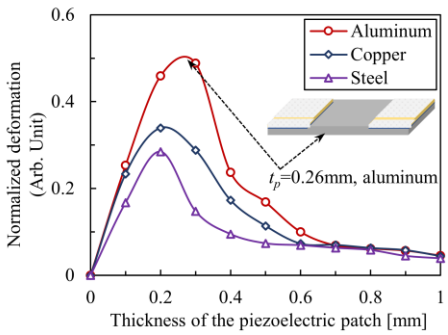

Fig. 3. Relationship of the thickness of the piezoelectric patch, t_p, to the normalized deformation amplitude
(l_p=35mm, where the red circles, blue squares and purple triangles represent different materials used for the vibrating plate, aluminum, copper and steel, respectively)

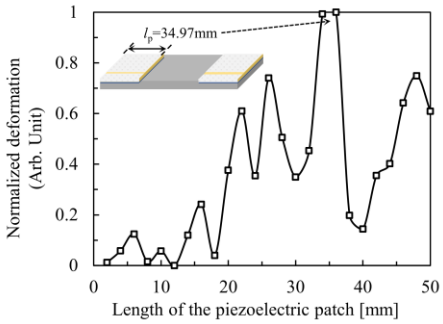

Fig. 4. Value of the normalized Z-directional deformation to the length of the piezoelectric patches, l_p
(t_p=0.26mm, aluminum being chosen as the material of the vibrating plate)

The value of t_p was varied from 0 to 1 mm (using an interval of 0.1 mm), and the maximum amplitude, over the vibrating plate of the robot, was determined through modal analysis. The results of the simulation carried out and giving the values of the amplitudes are shown in Fig. 3, which illustrates its relationship with t_p. It can be noted that at t_p=0.26 mm, the amplitude of the vibrating plate (aluminum) reaches its maximum.

TABLE I
THE STRUCTURAL PARAMETERS OF THE SELF-DRIVEN ROBOT (UNIT, MM)

Symbol	Quantity	Size
L+2d	total length of the vibrating plate	100
b	width of the vibration plate / the piezoelectric patches	17
t_m	thickness of the vibrating plate	0.5
l_p(=2d)	length of the two piezoelectric ceramic patches	35
t_p	thickness of the two piezoelectric ceramic patches	0.26

Subsequently, the length of the piezoelectric ceramic patch, l_p, was varied between 2 mm and 50 mm, in 1 mm steps. The

simulation results showed that at l_p =34.97 mm, the maximum value of the amplitude in the z-direction was reached, as shown in Fig. 4 - a result which is highly consistent with the empirical length value chosen, of 35 mm. The structural parameters of the self-driven robot, determined from the FE analysis, are shown in Table I.

IV. FE Validation of the Generation of the TWs

It can be seen from Section II that there are two ways to change the direction of the TWs. In the first method, the direction can be changed periodically, whenever *f* varies across each modal frequency, and furthermore there exists a pure TW frequency, f_{TW}, between the two modal frequencies. Alternatively, the direction of the TWs on the vibrating plate can be changed when θ exceeds 180° when using the second method, and so there exist two temporal phase shifts, θ_1 and θ_2, where the pure TWs, in both propagation directions, could be produced.

A. *f*-changing based approach

In order to demonstrate the effectiveness of the *f*-changing based approach, a model of the piezoelectric robot was first established using FE analysis according to the structural parameters listed in Table 1, and subsequently this model was analyzed to obtain the three adjacent modal frequencies, f_{10}=16.580kHz, f_{11}=19.333kHz, f_{12}= 24.059kHz, corresponding to the 10th, 11st and 12nd modes. The simulated values of the modal frequency were approximately in accordance with the theoretical results obtained from (3) and Fig. 2. By substituting these frequencies, f_{10}, f_{11}, f_{12}, into (8), two pure TW frequencies, f_{TW1}=18.005kHz and f_{TW2}=21.824kHz, were determined.

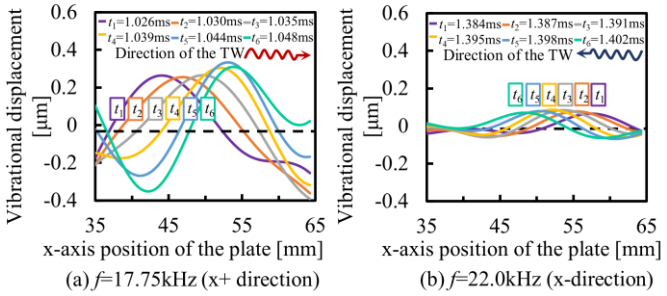

Fig. 5. Transient simulation results of the TW vibrational displacement along the plate, using the *f*-changing based approach (V_{pp}=10V, θ=90°, lines with different color in the graph represent waveforms at different times)

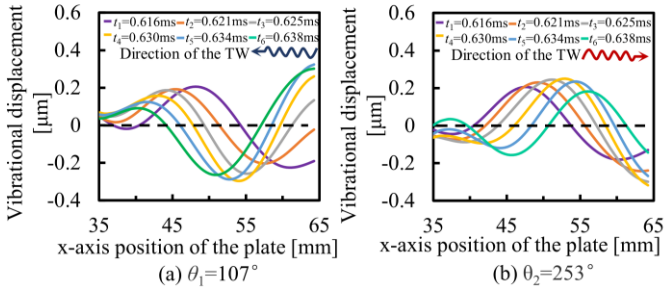

Fig. 6. Transient simulation results of the TW vibrating displacement along the plate, using the θ programming method (V_{pp}=10V, *f*=18.250kHz, lines with different color in the graph represents waveforms at different times)

Subsequently, in order to verify that TWs could be generated, transient simulations were performed at these two TW frequencies. Specifically, the two sinusoidal excitation signals with an $V_{peak\text{-}peak}$ amplitude of 10V and 90° phase shift were applied to the two piezoelectric patches. As a result, the components of the two TWs reached their maximum when the patches were excited at frequencies of 17.75 kHz and 22.00 kHz respectively, and the directions of the two TWs were opposite to each other. The displacements on the middle part of the vibrating plate (which is not covered by the piezoelectric patches at each end, these ranging from 35 mm to 65 mm) were acquired, corresponding to six different times each having an approximate interval of 5μs ($t_1 \sim t_6$), which are plotted in Fig. 5. At f_{TW1}=17.75kHz and at f_{TW2}=22.00kHz, the *x*+ and *x*- direction TWs is propagated, and the maximum z-directional displacement amplitude reached 0.3 μm and 0.1μm respectively. As can be seen, a deviation between the theoretically calculated values of f_{TW1}, and f_{TW2} and the simulated frequencies occurs. This is because only two adjacent modes were considered using (8), while the influence of other modes on the TWs was not considered. In addition, a large fluctuation seen in the *z*-direction amplitude at the two pure TW frequencies was caused by different modal amplitudes, so it is difficult to smoothly adjust the motion of the robot using this *f*-based method.

B. θ-changing based approach

As can be seen from Fig. 5, it is difficult to control the velocity smoothly and stabilize the amplitudes of the TWs using the above-mentioned *f*-based method while, by comparison, the θ-based method shows several advantages. To verify this, the same model was used in the FE simulation, but the temporal phase shift of the excitation signals applied to the two piezo ceramic patches, θ, varied from 0° to 360°, at a given frequency of 18.250 kHz. The superpositioned wave forms of the TW vibration obtained at θ_1=107° and θ_2=253° were extracted and plotted in Fig. 6 (as graphs (a) and (b) respectively), where the TW component reached the maximum. This also indicates a simulated spatial phase difference, φ, of 287°, which garantees the amplitude of the TW according to (12). In these curves formed using the θ programming method, the propagating directions of the TWs are opposite to each other and the displacement amplitudes in the *z*-direction are both ~0.2 μm. This condition allows for a smoother control of the self-running piezoelectric robot, compared to that using the *f*-based method.

V. Experimental Verification

A. System Configuration

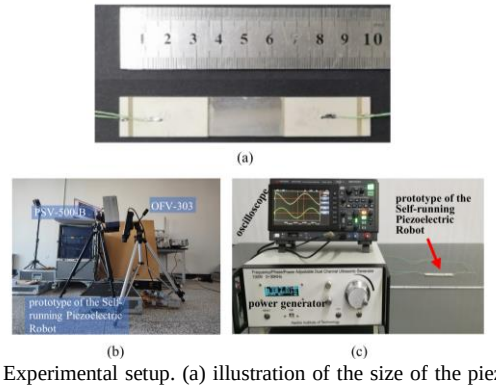

Fig. 7. Experimental setup. (a) illustration of the size of the piezoelectric robot (with reference to a ruler) (b) measurement of the vibrational

characteristics (c) test motional characteristics of the self-running piezoelectric robot developed (total length: 100 mm)

The piezoelectric robot prototype was fabricated as shown in Fig. 7(a), according to the structure dimensions set out in Table I, whose dimensions were identical to those of the simulation model. It can be seen that two piezoelectric ceramic patches (PZT-5A, fold-back electrodes type) were glued to an aluminum alloy vibrating plate (type 5052, Chinese standard) using epoxy adhesive.

In order to test its characteristics, i.e., the component and direction of the TWs being propagated along the self-running prototype, a test setup to evaluate the vibration was created, as shown in Fig. 7(b). The prototype was excited by a small voltage ($V_{peak\text{-}peak}$=10V), and the amplitude and phase of the vibrational velocity in the *z*-direction were measured using a scanning Laser Doppler Vibrometer (LDV, PSV-500-B type, Polytec).

Following that, in order to measure the characteristics of the motion of the prototype, the two piezoelectric ceramic patches glued to the prototype were connected to a power generator developed by the authors [42] (dual channel, 200W, 0-120V, 0-100kHz, 0-360°). As it was limited by the output voltage of the power generator, the Near Field Acoustic Levitation (NFAL) effect was ignored. During the experiments carried out, the two outputs of the ultrasonic power supply were adjusted to control the speed of movement of the prototype, this being recorded by using a digital camera (ILCE-6400, Sony, 120 Frames Per Second) and the speed was calculated from the video images with reference to a ruler glued to the ground - the experimental platform that was built is shown in Fig. 7(c).

B. Experimental verification of the f-changing and θ-changing approaches to adjust the direction of motion

The effectiveness of both the θ-changing and *f*-changing based approaches have been analyzed by using the FE simulations discussed in Section IV. Following that, the effectiveness of both methods was experimentally explored. The values of the speed of the robot in motion were measured by varying both *f* and θ respectively.

1) Experiments using the *f*-changing approach

To verify the effectiveness of the *f*-based approach to control the direction of the motion, the relationship between the excitation frequency and the speed of movement of the piezoelectric robot over the tempered glass surface was measured. In the experiment, the peak - peak voltages ($V_{peak\text{-}peak}$) and the temporal phase shift of the power generator were set to 45V and 90°, respectively. In addition, the excitation frequency was varied between two adjacent modal frequencies, from 16.00 kHz to 17.20 kHz. The results obtained were plotted in Fig. 8(a), where the black dotted line and the red line represent the motion speed and the theoretical SWR value respectively, shown against the change in the excitation frequency, *f*. Furthermore, the prototype stopped moving at the two modal frequencies of 16.00 kHz and 17.20 kHz, revealing that only pure SWs existed on the vibrating plate, where the value of the SWR reaches its maximum. By comparison, the speed of the prototype reached its peak, 13.19 mm/s, when *f* had the value of the root mean square of the two adjacent modal frequencies. Here 16.50 kHz is close to the theoretically calculated TW frequency of 16.61 kHz (according to (6) and (7)) and these experimentally and theoretically determined TW frequencies are also shown in Fig. 8(a). However, when the excitation frequency is smaller than 16.00 kHz or greater than 17.20 kHz, although the direction of the TW changes, the excitation frequency deviates from the resonant frequency of the piezoelectric ceramic itself. This then results in a small vibration amplitude, where the robot stopped moving, which limits the potential of the *f*-based motion control approach considered here.

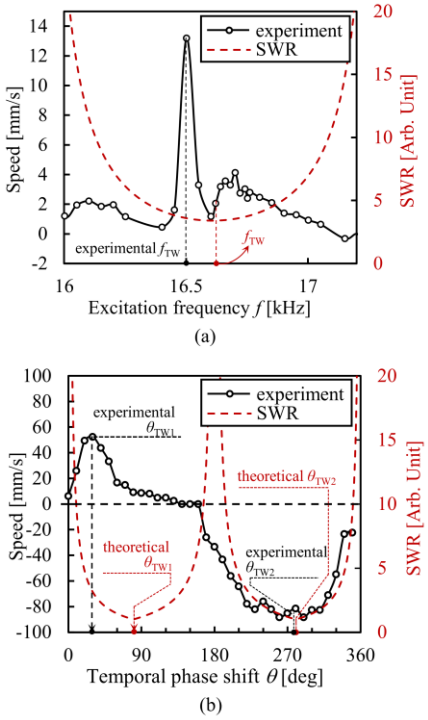

(a) The relationship between the excitation frequency, *f* , and the experimental speed of motion (black dotted line), or the theoretical value of the SWR (red dash line). ($V_{peak\text{-}peak}$ = 45V, θ was fixed at 90°)

(b) The relationship between the speed of motion and the temporal phase shift θ, where the black line and the red line represent the experimental speed and the theoretical value of the SWR of the robot, respectively. ($V_{peak\text{-}peak}$ =45V, *f*=16.273kHz)

Fig. 8. Comparison of the theoretical value of the SWR and the experimental results of the speed of motion of the self-running piezoelectric robot using both the *f*-based and θ-changing approach.

2) Experiments using the θ-changing approach

As can be seen from Fig. 6 (graphs (a) and (b)), the θ-based approach allows the speed of motion to be controlled more smoothly (by comparison to the *f*-based approach), because the excitation frequency has been fixed at the resonant frequency and the vibrational amplitudes show a smaller change. In order to verify experimentally the effectiveness of the speed control method based on programming θ, two excitation signals (where $V_{peak\text{-}peak}$ was 45V and the frequency used was 16.273kHz – this being the resonant frequency of the robot prototype) were applied to the piezoelectric self-running robot. When θ was adjusted from 0° to 360° (in intervals of 10°), the prototype moved on the tempered glass, and the relationship between the variational speed of the prototype and θ is shown in Fig. 8(b). The experimental and theoretical temporal phase shifts, θ_{TW1} and θ_{TW2}, (where the TW components were maximized on the vibrating plate), are shown in black and red in Fig. 8(b), respectively.

Fig. 8(b) reveals that the prototype moved along the x+ direction when θ was adjusted between 0° and 160°. However, the prototype moved along x- direction when θ ranged from 160° to 360°. Further, the maximum speed was reached when θ was ~30° and ~260°, which is essentially consistent with the theoretical and simulation results shown in Fig. 2(b) and Fig. 6. Therefore, the control method based on programming θ is verified as the most effective. Additionally, the x+ directional speed of the prototype is significantly lower than the x-directional speed, and its direction of movement changed when θ exceeded 160° - so it can be seen that these ranges are not strictly symmetric about π (180°). This asymmetry is caused by the inconsistencies that occur during the assembly of the two piezoelectric ceramic patches in the prototype constructed.

C. Experimentation on the motion characteristics of the piezoelectric robot using the θ-changing based approach

1) Measurement of the TW-vibrational characteristics

Pure TWs can be formed along the vibrating plate, since the SWR is a function of θ under a given excitation frequency, according to (10). In practice, for the dual patch-type robot with length, (L+2d), the motional speed of the prototype can be controlled by adjusting θ, at a certain fixed excitation frequency, f.

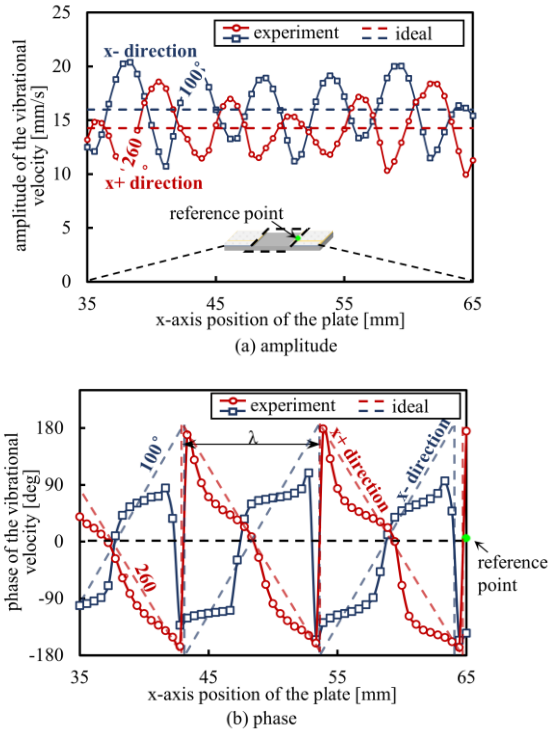

Fig. 9. The amplitudes and phase of the vibrational velocity along the vibrating plate corresponding to the two pure TWs along the two directions. (where the blue and red colored lines represent θ=100° and θ=260°, respectively; the solid and dashed lines are experimental and ideal results. Vpeak-peak=10V, f=16.273kHz, θ_1=100°, θ_2=260°, φ being calculated as 280°.)

During the experiments carried out in this work, f was set to be 16.273 kHz, and the two temporal phase shifts corresponding to the pure TWs in the x- and x+ directions, θ_1 and θ_2, could be found at 100° and 260° respectively. Specifically, the amplitude of the vibrational velocity distributed on the plate, corresponding to θ_1 and θ_2 (which was obtained from the scanning LDV) are shown in Fig. 9(a). As can be seen, the amplitude of the vibrational velocity was kept as ~15 mm/s, indicating that TWs have been formed along the plate, due to the value of the SWR being small (the values are 1.90 and 1.86, in the x- and x+ directions respectively). It is important to note that the vibrational velocities fluctuated by ~25% in the two cases, where the slight fluctuation seen may be caused by factors such as the differences between the connection of the two patches and the plate, and the asymmetry of the two patches used, for example in relation to their clamped capacitances, mechanical quality factors, etc.

In order to understand better the directions of the TWs, the phase of the vibrational velocity could be used, according to the TW expression given in (12). To do so, a single point LDV (OFV-303, Polytec) was connected as an input for the reference point of zero phase, this being marked green on both Fig. 9(a) and Fig. 9(b). The phase of the vibrational velocity increased (θ_1=100°) or decreased (θ_2=260°) periodically between -180° and 180° with respect to the wavelength, λ, which indicated the opposite directions of propagation of the TWs.

2) Measurement of the characteristics of the robot motion

Measurement of the velocity-voltage relationship: Two sinusoid signals, of the same amplitude and frequency, 16.273kHz, were applied to the two patches of the prototype robot. Here the temporal phase shifts were set to θ_1=100° and θ_2=260°, corresponding to the two TWs in the x+ and x-directions. In addition, the peak-to-peak value of the excitation voltage was adjusted from 5 V to 50 V, in intervals of 5 V. As a result, the relationship between the velocity of motion of the prototype running on a tempered glass plate, v, and the peak-to-peak value of the excitation signal, $V_{peak\text{-}peak}$, in Fig. 10(a).

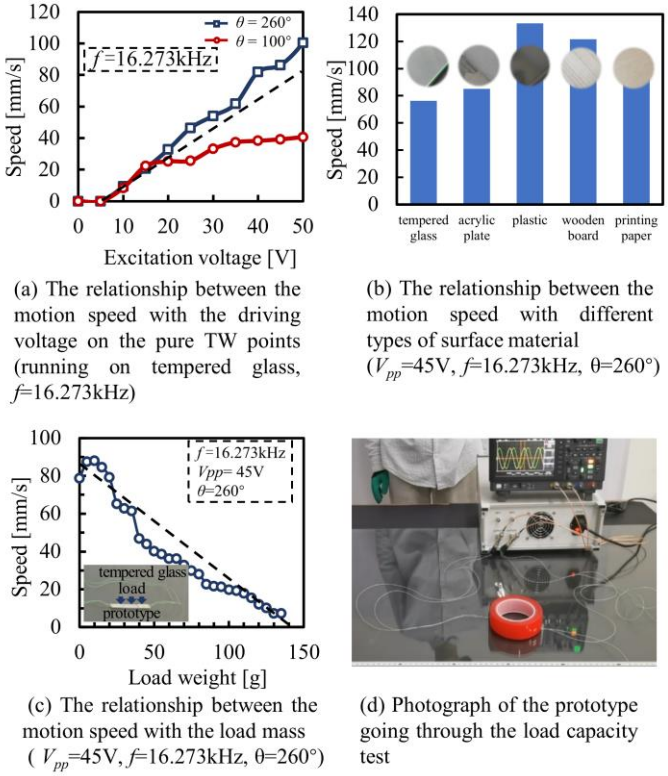

(a) The relationship between the motion speed with the driving voltage on the pure TW points (running on tempered glass, f=16.273kHz)

(b) The relationship between the motion speed with different types of surface material (V_{pp}=45V, f=16.273kHz, θ=260°)

(c) The relationship between the motion speed with the load mass (V_{pp}=45V, f=16.273kHz, θ=260°)

(d) Photograph of the prototype going through the load capacity test

Fig. 10. Measurement of the characteristics of the motion of the self-running piezoelectric robot

Table II
PERFORMANCE COMPARISONS WITH SOME PREVIOUS PIEZOELETRIC ROBOTS

Indicator [unit]	This study	Son et al. [7]	Hariri 2016 [8]	Chen et al [9]	Hariri 2013 [32]
weight[g]	6g	23.25	6.27	20.13g	6.45
Max speed[cm/s]	10	5.86	30.2	1.65	13.1
Voltage peak-peak[V]	50	20	200	200	60
Payload [g]	151.7	-	-	80	18
Dimension [mm*mm*mm]	100*17*0.76	53 x 45 x 19	50 x 10 x 10.5	-	180 x 17 x 0.77
Frequency [kHz]	16.273	24.7	2.4/3.1	21.07	11.3

It can be seen from Fig. 10(a) that the motional velocity of the robot increases with the excitation voltage, and v shows an approximate linear relationship with $V_{peak\text{-}peak}$. However, even though the same $V_{peak\text{-}peak}$ voltage was applied to the piezoelectric patches of the vibrating plate, the velocity at θ_1=260° was much higher than that at θ_2=100°, this possibly being caused by the asymmetrical position that occurred when the two patches were being glued. It should be noted that the robot has a 'deadband' drive voltage, of about 5 V in both directions, which was caused by the static friction force between the robot and the glass substrate.

Evaluation of performance on different material surfaces: The motion of the self-running robot on different material surfaces has also been tested ($V_{peak\text{-}peak}$ = 45V, f = 16.273kHz, θ = 260°), to evaluate its adaptability to different terrains. In this test, five different types of materials were used: tempered glass, acrylic board, thin film crystal, wooden board (with a wax treatment) and printing paper (surface roughness (RA) being sorted from small to large). The results of the measurement of the velocity are illustrated in Fig. 10(b), which shows that the piezoelectric self-running robot has a very definite ability to adapt to different complex environments.

In relation to the friction wear problem, in a travelling wave robot the friction occurs over the whole contact surface, but in a standing wave robot, the friction only occurs at the nodal points and therefore the friction wear problem is reduced, which is an advantage with this type of robot.

Evaluation of the load capacity of the robot: Knowing the load carrying ability of the robot is critical, as it can limit the range of its applications. Therefore, the maximum velocity of the prototype was measured under different loads being placed to the center of the robot. The experiments were conducted when $V_{peak\text{-}peak}$ was set to 45 V, f and θ were made equal to 16.273 kHz and 260° respectively. The weight of the prototype itself (before loading) was 6.0 g. Different weights, ranging from 5 g and up to a maximum of 135 g (applied in 5 g intervals) were loaded on the robot and its performance evaluated.

The characteristic relationship between the robot velocity and the load carried, for this prototype, is shown in Fig. 10(c), from which it can be seen that the velocity of the prototype on the tempered glass plate reached its maximum when a load of 10 g was used. The main reason for this phenomenon is as follows – the load mass, of between 0-10g, can be seen as providing a preload force between the prototype and the tempered glass, where the load mass of 10g used provides the optimal preload force, so that the prototype and the bottom have the best preload to maximizes the driving force. However, as the load continues to increase, the robot needs to overcome the greater friction experienced and the velocity with which it then moves decreases as a result. The experimental platform for the load test carried out is shown in Fig. 10(d), where the red tape (having a weight of 151.7 g), could be dragged slowly by the self-running piezoelectric robot. This means that the robot can carry at least 26 times its own weight and thus has an excellent load carrying capability.

D. Performance Comparisons

A comparison of the performance characteristics and design of the device proposed in this work with those of a number of self running piezoelectric robots is illustrated in Table II. In summary, this has shown that the robot reported in this work achieved a relatively fast speed, while its load carrying ability is higher than that of the design of Chen et al [9] and Hariri et al [32]. Furthermore, the weight and size of the proposed robot is lower than that of Son et al [7] and Hariri et al [8] – this showing the advantages of having a simple structure and as well the potential for use in applications in confined spaces.

VI. CONCLUSION

In this work, two methods to create program-based control of the direction and component of the TWs have been presented. To understand better the TW and SW parts of the vibrational displacement seen, the expression for the z-direction displacement of the vibrating plate was deduced. As a result, both f-based and θ-based methods to control the Standing Wave Ratio (SWR) have been described.

Prior to the experiments being carried out, Finite Element Analysis based simulations were used to optimize the size of the self-running piezoelectric robot, in order to improve its velocity of motion and load capacity. As a result, the optimized structural dimensions were 100mm x 17mm x 0.5mm, and the size of the piezoelectric patches used was 35mm x 17mm x 0.26mm. Then, by using transient simulation, the TWs with opposite directions were determined using both approaches, but the vibrational displacement of the θ-based method was seen to be smoother than using the f-based approach. In the experiments undertaken, a 100mm long prototype was developed and the values of f and θ were separately adjusted, between 16.0 kHz and 17.2 kHz, and 0 and 2π (360°) respectively. The results obtained have revealed that both methods could allow the adjustment of the direction and composition of the TWs, but the prototype moved more smoothly and had a higher velocity, using the θ-based approach.

Finally, the velocity of motion and the load-bearing characteristics of the self-running piezoelectric robot were tested and evaluated, in addition to its adaptability to different terrains.

REFERENCES

[1] A. Ferreira, and J.-G. Fontaine, "Dynamic modeling and control of a conveyance microrobotic system using active friction drive," *IEEE-ASME Trans. Mechatron.*, vol. 8, no. 2, pp. 188-202, Jun. 2003.

[2] A. Abadi, and G. Kosa, "Piezoelectric beam for intrabody propulsion controlled by embedded sensing," *IEEE-ASME Trans. Mechatron.*, vol. 21, no. 3, pp. 1528-1539, Jun. 2016.

[3] L. Jones et al., "Vehicle propulsion by solid state motion." in *Proc. ASME Smart Mater., Adaptive Struct. Intell. Syst.*, Sep. 8-10, 2014.

[4] G. Kosa, M. Shoham, and M. Zaaroor, "Propulsion method for swimming microrobots," *IEEE Trans. Robot.*, vol. 23, no. 1, pp. 137-150, Feb. 2007.

[5] X. Zhou et al., "Development of an Anti-Hydropressure Miniature Underwater Robot with Multi-Locomotion Mode Using Piezoelectric Pulsed-Jet Actuator," *IEEE Trans. Ind. Electron.*, 2022.

[6] X. Li, P. Ci, G. Liu, and S. Dong, "A two-layer linear piezoelectric micromotor," *Ultrason. Ferroelectr. Freq. Control.*, vol. 62, no. 3, pp. 405-411, Mar. 2015.

[7] K. J. Son, V. Kartik, J. A. Wickert, and M. Sitti, "An ultrasonic standing-wave-actuated nano-positioning walking robot: Piezoelectric-metal composite beam modeling," *J. Vib. Control*, vol. 12, no. 12, pp. 1293-1309, Dec. 2006.

[8] H. H. Hariri, L. A. Prasetya, S. Foong, G. S. Soh, K. N. Otto and K. L. Wood, "A tether-less Legged Piezoelectric Miniature Robot using bounding gait locomotion for bidirectional motion," *2016 IEEE International Conference on Robotics and Automation (ICRA)*, Stockholm, Sweden, May 16-21, 2016.

[9] K. Chen, S. Gao, Y. Pan, and P. Guo, "Self-running and self-floating two-dimensional actuator using near-field acoustic levitation," *Appl. Phys. Lett.*, vol. 109, no. 12, pp. 123503, Sep. 2016.

[10] D. Avirovik, B. Butenhoff, and S. Priya, "Millipede-inspired locomotion through novel U-shaped piezoelectric motors," *Smart Mater. Struct.*, vol. 23, no. 3, pp. 037001, Feb. 2014.

[11] P. Ci, G. Liu, Z. Chen, and S. Dong, "A standing wave linear ultrasonic motor operating in face-diagonal-bending mode," *Appl. Phys. Lett.*, vol. 103, no. 10, pp. 102904, Sep. 2013.

[12] S. C. Shen, and Y. C. Chen, "Design and Evaluation of a Multi-degree-of-freedom Piezoelectric Microactuator and its Applications," *Int. J. Autom.Smart Technol.*, vol. 3, no. 4, pp. 251-257, Dec. 2013.

[13] J. Wu, Y. Mizuno, and K. Nakamura, "Polymer-based ultrasonic motors utilizing high-order vibration modes," *IEEE-ASME Trans. Mechatron.*, vol. 23, no. 2, pp. 788-799, Apr. 2018.

[14] J. Li, H. Huang, and T. Morita, "Stepping piezoelectric actuators with large working stroke for nano-positioning systems: a review," *Sens. Actuator A-Phys.*, vol. 292, pp. 39-51, Jun. 2019.

[15] J. Wu et al., "A Two-DOF linear ultrasonic motor with high thrust force density and high power density utilizing torsional/centrosymmetric-bending/ symmetric-bending Modes," *IEEE Trans. Ind. Electron.*, vol. 69, no. 8, pp. 8220-8230, Aug. 2022.

[16] J. Deng, Y. Liu, J. Li, S. Zhang and K. Li, "Displacement Linearity Improving Method of Stepping Piezoelectric Platform Based on Leg Wagging Mechanism," *IEEE Trans. Ind. Electron.*, vol. 69, no. 6, pp. 6429-6432, June 2022.

[17] P. Smithmaitrie, P. Suybangdum, P. Laoratanakul, and N. Muensit, "Design and performance testing of an ultrasonic linear motor with dual piezoelectric actuators," *Ultrason. Ferroelectr. Freq. Control.*, vol. 59, no. 5, pp. 1033-1042, May, 2012.

[18] H. Peng, J. Yang, X. Lu, P. Zhu and D. Wu, "A Lightweight Surface Milli-Walker Based on Piezoelectric Actuation," *IEEE Trans. Ind. Electron.*, vol. 66, no. 10, pp. 7852-7860, Oct. 2019.

[19] H. Hariri, Y. Bernard, and A. Razek, "2-D traveling wave driven piezoelectric plate robot for planar motion," *IEEE-ASME Trans. Mechatron.*, vol. 23, no. 1, pp. 242-251, Feb. 2018.

[20] H. Hariri, Y. Bernard, and A. Razek, "Dual piezoelectric beam robot: The effect of piezoelectric patches' positions," *J. Intell. Mater. Syst. Struct.*, vol. 26, no. 18, pp. 2577-2590, Feb. 2015.

[21] Y. Liu, W. Chen, J. Liu and X. Yang, "A High-Power Linear Ultrasonic Motor Using Bending Vibration Transducer," *IEEE Trans. Ind. Electron.*, vol. 60, no. 11, pp. 5160-5166, Nov. 2013.

[22] R. Gabai, R. Shaham, S. Davis, N. Cohen, and I. Bucher, "A Contactless Stage Based on Near-Field Acoustic Levitation for Object Handling and Positioning—Concept, Design, Modeling, and Experiments," *IEEE-ASME Trans. Mechatron.*, vol. 24, no. 5, pp. 1954-1963, Oct. 2019.

[23] D. Koyama, and K. Nakamura, "A self-running ultrasonically levitated 2D stage using flexural vibrating plates," *Phys. Procedia*, vol. 3, no. 1, pp. 1047-1052, Jan. 2010.

[24] G. Kim, J. Park, and S. Jeong, "Analysis of dynamic characteristics for vibration of flexural beam in ultrasonic transport system," *J. Mech. Sci. Technol.*, vol. 23, no. 5, pp. 1428-1434, May. 2009.

[25] M. Kuribayashi, S. Ueha, and E. Mori, "Excitation conditions of flexural traveling waves for a reversible ultrasonic linear motor," *J. Acoust. Soc. Am.*, vol. 77, no. 4, pp. 1431-1435, Apr. 1985.

[26] Y. Hashimoto, Y. Koike, and S. Ueha, "Transporting objects without contact using flexural traveling waves," *J. Acoust. Soc. Am.*, vol. 103, no. 6, pp. 3230-3233, May, 1998.

[27] D. Koyama, K. Nakamura, and S. Ueha, "A stator for a self-running, ultrasonically-levitated sliding stage," *Ultrason. Ferroelectr. Freq. Control.*, vol. 54, no. 11, pp. 2337-2343, Nov. 2007.

[28] A. Minikes, R. Gabay, I. Bucher, and M. Feldman, "On the sensing and tuning of progressive structural vibration waves," *Ultrason. Ferroelectr. Freq. Control.*, vol. 52, no. 9, pp. 1565-1576, Sep. 2005.

[29] V. Malladi, D. Avirovik, S. Priya, and P. Tarazaga, "Characterization and representation of mechanical waves generated in piezo-electric augmented beams," *Smart Mater. Struct.*, vol. 24, no. 10, pp. 105026, Sep. 2015.

[30] D. Avirovik, V. S. Malladi, S. Priya, and P. A. Tarazaga, "Theoretical and experimental correlation of mechanical wave formation on beams," *J. Intell. Mater. Syst. Struct.*, vol. 27, no. 14, pp. 1939-1948, Feb. 2016.

[31] B.-G. Loh, and P. I. Ro, "An object transport system using flexural ultrasonic progressive waves generated by two-mode excitation," *Ultrason. Ferroelectr. Freq. Control.*, vol. 47, no. 4, pp. 994-999, Jul. 2000.

[32] H. Hariri, Y. Bernard, and A. Razek, "A traveling wave piezoelectric beam robot," *Smart Mater. Struct.*, vol. 23, no. 2, pp. 025013, Dec. 2013.

[33] B. Dehez, C. Vloebergh, and F. Labrique, "Study and optimization of traveling wave generation in finite-length beams," *Math. Comput. Simul.*, vol. 81, no. 2, pp. 290-301, May, Oct. 2010.

[34] R. Gabai, and I. Bucher, "Excitation and sensing of multiple vibrating traveling waves in one-dimensional structures," *J. Sound Vib.*, vol. 319, no. 1-2, pp. 406-425, Jan. 2009.

[35] G. Mu, J. Zhao, H. Dong, J. Wu, K. T. V. Grattan, and T. Sun, "Structural parameter study of dual transducers-type ultrasonic levitation-based transportation system," *Smart Mater. Struct.*, vol. 30, no. 4, pp. 045009, Feb. 2021.

[36] J. Wu et al., "Development of a Self-Moving Ultrasonic Actuator with High Carrying/Towing Capability Driven by Longitudinal Traveling Wave," *IEEE-ASME Trans. Mechatron.*, 2022.

[37] K. F. Graff, *Wave motion in elastic solids*. New York: Dover, 1991.

[38] O. Koyama, D. Koyama, K. Nakamura, and S. Ueha, "Ultrasonic linear motor using traveling vibration on fine ceramic twin ridges," *Acoust. Sci. Technol.*, vol. 29, no. 1, pp. 95-98, Jan. 2008.

[39] Y. Tomikawa, K. Adachi, H. Hirata, T. Suzuki, and T. Takano, "Excitation of a progressive wave in a flexurally vibrating transmission medium," *Jpn. J. Appl. Phys.*, vol. 29, no. S1, pp. 179, 1990.

[40] J. Zhao, G. Mu, H. Dong, T. Sun, and K. T. Grattan, "Requirements for a transportation system based on ultrasonic traveling waves using the measurement of spatial phase difference," *Mech. Syst. Signal Proc.*, vol. 168, pp. 108708, Apr. 2022.

[41] Y. Liu, J. Yan, L. Wang and W. Chen, "A Two-DOF Ultrasonic Motor Using a Longitudinal–Bending Hybrid Sandwich Transducer," *IEEE Trans. Ind. Electron.*, vol. 66, no. 4, pp. 3041-3050, Apr. 2019.

[42] H. Dong, J. Wu, G. Zhang, and H. Wu, "An improved phase-locked loop method for automatic resonance frequency tracing based on static capacitance broadband compensation for a high-power ultrasonic transducer," *Ultrason. Ferroelectr. Freq. Control.*, vol. 59, no. 2, pp. 205-210, Feb. 2012.

Biographical notes

JIE ZHAO (M'05) was born was born in Jilin, China, in 1968. He received the B.E., M.E., and Ph.D. degrees from the Harbin Institute of Technology, Harbin, China, in 1990, 1993, and 1996, respectively.

He has been a Professor with the State Key Laboratory of Robotics and System, Harbin Institute of Technology, Harbin, China, since 2001. His research interest includes design, modeling and control of industrial robots and bionic robots.

Prof. Zhao is the Leader of the Subject Matter Expert Group of Intelligent Robot in National 863 Program supervised by the Ministry of Science and Technology of China.

GUANYU MU was born in Heilongjiang, China, in 1993. He received the B.E. degree in mathematics and applied mathematics in 2015, the M.E. degree in industrial engineering in 2018, from the Sino-French Engineer School of Beihang University, Beijing, China. Currently, he is a Ph.D. candidate in the School of Mechatronics Engineering, Harbin Institute of Technology, Harbin, China.

His research project focuses on high-power ultrasonic technology, piezoelectric transducers and actuators, and acoustic levitation-based transportation.

HUIJUAN DONG was born in Henan, China, in 1968. She received the B.E. degree in precise mechanical engineering and the master's and Ph.D. degrees in mechatronics engineering from the Harbin Institute of Technology, Harbin, China, in 1990, 1996, and 1999, respectively.

She joined in Harbin Institute of Technology in 1997. Subsequently, she was promoted to an Associate Professor in 2001, and a Full Professor in 2012. Her research project focuses on acoustics.

KENNETH THOMAS VICTOR GRATTAN was born in Lurgan, U.K., in 1953. He received the B.Sc. degree (Hons.) in physics and the Ph.D. degree in laser physics from Queen's University Belfast, in 1974.

He became a Research Fellow of the Imperial College of Science and Technology, in 1978. In 1983, he joined the City University of London as a new blood Lecturer in physics being appointed as a Professor of measurement and instrumentation, in 1991, and the Head of the Department of Electrical, Electronic, and Information Engineering. From 2001 to 2008, he was the Associate and then the Deputy Dean of the School of Engineering, from 2008 to 2012, and the First Conjoint Dean of the School of Engineering and Mathematical Sciences and the School of Informatics. In 2013, he was appointed as the Inaugural Dean of the City Graduate School. His research interests have expanded to the measurement of a range of physical and chemical parameters using optical methods.

Prof. Grattan was appointed as a George Daniels Professor of scientific instrumentation, in 2013, and the Royal Academy of Engineering Research Chair, in 2014. He was elected to the Royal Academy of Engineering, the U.K. National Academy of Engineering, in 2008.

Tong Sun was born in Jiangsu, China in 1968. She was awarded the degrees of Bachelor of Engineering, Master of Engineering and Doctor of Engineering from the Department of Precision Instrumentation of Harbin Institute of Technology, Harbin, China in 1990, 1993 and 1998, respectively. She was awarded the degree of Doctor of Philosophy at City University in applied physics in 1999.

She was an Assistant Professor at Nanyang Technological University in Singapore from year 2000 to 2001 before she re-joined City University in 2001 as a Lecturer. Subsequently she was promoted to a Senior Lecturer in 2003, a Reader in 2006 and a Professor in 2008 at City University, London. Her research project focuses on developing a range of optical fiber sensors.